

1 Mineralization of the recalcitrant oxalic and oxamic  
2 acids by electrochemical advanced oxidation processes  
3 using a boron-doped diamond anode

4 Sergi Garcia-Segura, Enric Brillas\*

5 *Laboratori d'Electroquímica de Materials i del Medi Ambient, Departament de Química*  
6 *Física, Facultat de Química, Universitat de Barcelona, Martí i Franquès 1-11, 08028*  
7 *Barcelona, Spain*

8 *Paper submitted to be published in Water Research*

9 \*Corresponding author: Tel.: +34 93 4021223; Fax: +34 93 4021231

10 *E-mail address: brillas@ub.edu*

## 11 **Abstract**

12 Oxalic and oxamic acids are the ultimate and more persistent by-products of the degradation of  
13 *N*-heteroaromatics by electrochemical advanced oxidation processes (EAOPs). In this paper,  
14 the kinetics and oxidative paths of these acids have been studied for several EAOPs using a  
15 boron-doped diamond (BDD) anode and a stainless steel or an air-diffusion cathode. Anodic  
16 oxidation (AO-BDD) in the presence of  $\text{Fe}^{2+}$  (AO-BDD- $\text{Fe}^{2+}$ ) and under UVA irradiation (AO-  
17 BDD- $\text{Fe}^{2+}$ -UVA), along with electro-Fenton (EF-BDD), were tested. The oxidation of both  
18 acids and their iron complexes on BDD was clarified by cyclic voltammetry. AO-BDD  
19 allowed the overall mineralization of oxalic acid, but oxamic acid was removed much more  
20 slowly. Each acid underwent a similar decay in AO-BDD- $\text{Fe}^{2+}$  and EF-BDD, as expected if its  
21 iron complexes were not attacked by hydroxyl radicals in the bulk. The faster and total  
22 mineralization of both acids was achieved in AO-BDD- $\text{Fe}^{2+}$ -UVA due to the high  
23 photoactivity of their Fe(III) complexes that were continuously regenerated by oxidation of  
24 their Fe(II) complexes. Oxamic acid always released a larger proportion of  $\text{NH}_4^+$  than  $\text{NO}_3^-$   
25 ion, as well as volatile  $\text{NO}_x$  species. Both acids were independently oxidized at the anode in  
26 AO-BDD, but in AO-BDD- $\text{Fe}^{2+}$ -UVA oxamic acid was more slowly degraded as its content  
27 decreased, without significant effect on oxalic acid decay. The increase in current density  
28 enhanced the oxidation power of the latter method, with loss of efficiency. High  $\text{Fe}^{2+}$  contents  
29 inhibited the oxidation of Fe(II) complexes by the competitive oxidation of  $\text{Fe}^{2+}$  to  $\text{Fe}^{3+}$ . Low  
30 current densities and  $\text{Fe}^{2+}$  contents are preferable to remove more efficiently these acids by the  
31 most potent AO-BDD- $\text{Fe}^{2+}$ -UVA method.

32 *Keywords:* Carboxylic acids; Iron complexes; Anodic oxidation; Electro-Fenton; UVA light;  
33 Removal kinetics

## 34 1. Introduction

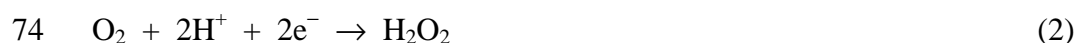
35 Recently, a large variety of advanced oxidation processes (AOPs) has been proposed for  
36 the remediation of wastewaters containing low contents of toxic and/or biorefractory organic  
37 pollutants (Andreozzi et al., 1999; Pera-Titus et al., 2004; Cañizares et al., 2008). These  
38 powerful oxidation methods include chemical, photochemical and electrochemical treatments  
39 based on the in situ generation of hydroxyl radical ( $\bullet\text{OH}$ ). This radical is the second most  
40 strong oxidizing specie known after fluorine with a high standard reduction potential  
41 ( $E^\circ(\bullet\text{OH}/\text{H}_2\text{O}) = 2.80 \text{ V vs. SHE}$ ) that allows its non-selectively reaction with most organics  
42 leading to their overall mineralization to  $\text{CO}_2$ , water and inorganic ions. However, the  
43 effectiveness of AOPs is limited by the formation of recalcitrant carboxylic acids (Cañizares  
44 et al., 2003; Oturan et al., 2008; Serra et al., 2009). The most common ultimate by-product  
45 from aromatics is oxalic acid, which is hardly destroyed with  $\bullet\text{OH}$  largely prolonging the  
46 mineralization time with the consequent efficiency loss and/or greater operation cost of the  
47 treatment (Brillas et al., 2004; Pera-Titus et al., 2004; Diagne et al., 2007; Özcan et al., 2008).  
48 In the degradation of wastewaters with *N*-aromatics, a mixture of oxalic and oxamic acids is  
49 finally formed (Sirés et al., 2006; Hammami et al., 2008; Hamza et al., 2009; Brillas et al.,  
50 2010). Oxamic acid is even more recalcitrant than oxalic acid (Faria et al., 2008). While the  
51 removal rate of oxalic acid is strongly enhanced in photoassisted AOPs with iron ions (Zuo  
52 and Hoigné, 1992; Faust and Zepp, 1993; Zuo and Hoigné, 1994; Šima and Makáňová, 1997),  
53 less is known about the mineralization of oxamic acid by photochemical treatments.

54 The most typical electrochemical AOP (EAOP) is anodic oxidation (AO) in which organic  
55 pollutants contained in an electrolytic cell can be oxidized at the anode surface either by direct  
56 charge transfer and/or with  $\bullet\text{OH}$  generated from water oxidation at high current. For a boron-  
57 doped diamond (BDD) electrode, the formation of hydroxyl radical can be written as reaction  
58 (1) (Marselli et al., 2003; Sirés et al., 2008; Panizza and Cerisola, 2009; Brillas et al., 2010):



60 The BDD electrode has a much higher oxidation power than other conventional anodes and it  
61 is able to effectively mineralize oxalic acid (Gandini et al., 2000; Martínez-Huitle et al., 2004;  
62 Vandini et al., 2006; Weiss et al., 2007; Scialdone et al., 2008), but no information is  
63 available on the AO treatment of oxamic acid. The high oxidation power of BDD also allows  
64 generating reactive oxygen species (ROS) like  $\text{H}_2\text{O}_2$  and ozone, as well as peroxy-derivatives  
65 coming from the oxidation of the anion of the background electrolyte (Cañizares et al., 2003;  
66 Panizza and Cerisola, 2009). In previous work (Guinea et al., 2009), we found that the  
67 presence of  $\text{H}_2\text{O}_2$  in AO accelerates the mineralization process of carboxylic acids, although  
68 Fe(III)-oxalate complexes are quickly photolyzed by UVA light.

69 EAOPs based on Fenton's reaction chemistry have been recently developed (Brillas et al.,  
70 2009). In electro-Fenton (EF),  $\text{H}_2\text{O}_2$  is continuously supplied to an acidic contaminated  
71 solution from the two-electron reduction of injected  $\text{O}_2$  at a carbonaceous cathode, mainly  
72 carbon felt (Oturán et al., 2008; Balci et al., 2009) and carbon-PTFE gas-diffusion electrodes  
73 (Sirés et al., 2007, Ruiz et al., 2011), by reaction (2):



75  $\text{Fe}^{2+}$  ion is then added to the solution to react with  $\text{H}_2\text{O}_2$  producing  $\bullet\text{OH}$  in the bulk and  $\text{Fe}^{3+}$   
76 by Fenton's reaction (3) (Sun and Pignatello, 1993):



78 An advantage of EF is that  $\text{Fe}^{2+}$  can be regenerated from  $\text{Fe}^{3+}$  reduction at the cathode,  
79 thus accelerating Fenton's reaction (3) and the oxidation of organics with  $\bullet\text{OH}$  (Brillas et al.,  
80 2009). When a one-compartment cell with a BDD anode is used, the degradation of organic  
81 pollutants is additionally enhanced by the attack of  $\text{BDD}(\bullet\text{OH})$  formed from reaction (1)  
82 (Serra et al., 2009; Ruiz et al. 2011). The mineralization of aromatics can also be accelerated

83 by exposing the contaminated solution to UVA light while is treated by EF (Brillas et al.,  
84 2004; Sirés et al., 2006; Ruiz et al., 2011). The main action of UVA irradiation is the  
85 photodecarboxylation of Fe(III)-carboxylate complexes.

86 The degradation of *N*-aromatics by EAOPs involves a high number of by-products that  
87 are simultaneously formed and destroyed by the different oxidizing species. Oxalic and  
88 oxamic acids are accumulated from the beginning of the process and their slow destruction  
89 limits the oxidation power of these methods. However, the influence of oxidants and/or UVA  
90 light on their removal, particularly of their iron species, is not well known yet.

91 To gain a better insight on the mineralization processes of oxalic and oxamic acids to  
92 better understand the degradation of *N*-aromatics, we report a study on the kinetics and  
93 oxidative paths of both acids by EAOPs with a BDD anode under typical treatment conditions  
94 of synthetic wastewaters with organics in sulfate medium. Special attention was taken on the  
95 action of Fe<sup>2+</sup> and UVA light to clarify the destruction of their iron complexes. The oxidation  
96 of these compounds on BDD was analyzed by cyclic voltammetry (CV). The change in  
97 degradation rate of each acid when mixed in different proportions was examined. The effect  
98 of current density and Fe<sup>2+</sup> content on oxamic acid removal was assessed. NH<sub>4</sub><sup>+</sup> and NO<sub>3</sub><sup>-</sup>  
99 ions lost during the mineralization of oxamic acid were followed by ionic chromatography.

## 100 **2. Materials and methods**

### 101 *2.1. Chemicals*

102 Oxalic and oxamic acids were of analytical grade from Avocado. Anhydrous sodium  
103 sulfate, ferrous sulfate heptahydrate and ferric sulfate hydrate were of analytical grade from  
104 Fluka and Sigma. Solutions were prepared with high-purity water obtained from a Millipore  
105 Milli-Q system with resistivity > 18 MΩ cm at 25 °C. Organic solvents and other chemicals  
106 used were of HPLC or analytical grade from Aldrich, Lancaster, Merck and Panreac.

## 107 2.2. Apparatus

108 The solution pH was measured with a Crison GLP 22 pH-meter. CV was conducted with  
109 an Ecochemie Autolab PGSTAT100 potentiostat-galvanostat controlled by an Autolab Nova  
110 1.5 software. Electrolyses were performed with an Amel 2053 potentiostat-galvanostat. The  
111 concentration of dissolved O<sub>2</sub> was determined with a Thermo Electron Corporation Orion 4  
112 Star pH-DO portable with a Sensor Orion 083005MD DO probe. Total organic carbon (TOC)  
113 of solutions was measured with a Shimadzu VCSN TOC analyzer. Total nitrogen (TN) was  
114 determined with a Shimadzu TNM-1 unit coupled with the TOC analyzer. The concentration  
115 of oxalic and oxamic acids was quantified by ion-exclusion HPLC using a Waters 600 liquid  
116 chromatograph fitted with a Bio-Rad Aminex HPX 87H, 300 mm × 7.8 mm (i.d.), column at  
117 35 °C, coupled with a Waters 996 photodiode array detector at  $\lambda = 210$  nm. Inorganic ions lost  
118 during oxamic acid degradation were detected by ionic chromatography using a Shimadzu 10  
119 Avp HPLC coupled with a Shimadzu CDD 10 Avp conductivity detector. NH<sub>4</sub><sup>+</sup> concentration  
120 was obtained with a Shodex IC YK-421, 125 mm × 4.6 mm (i.d.), cation column at 40 °C,  
121 whereas NO<sub>3</sub><sup>-</sup> content was determined with a Shim-Pack IC-A1S, 100 mm × 4.6 mm (i.d.),  
122 anion column at 40 °C.

## 123 2.3. Electrochemical systems

124 All electrolytic experiments were conducted in an open, undivided and thermostated  
125 cylindrical cell, so that all gases formed were directly released to the atmosphere. The anode  
126 was a BDD thin film provided by Adamant Technologies (La-Chaux-de-Fonds, Switzerland),  
127 while the cathode was either a stainless steel (AISI 304 grade) sheet (SS) or a carbon-PTFE  
128 air-diffusion electrode (ADE) from E-TEK (Somerset, NJ, USA). The preparation of the ADE  
129 cathode were described elsewhere (Brillas et al., 2004). It was fed with air pumped at 300 mL  
130 min<sup>-1</sup> to generate H<sub>2</sub>O<sub>2</sub> by reaction (2). The area of all electrodes was 3 cm<sup>2</sup> and the  
131 interelectrode gap was ca. 1 cm. To remove the impurities of the BDD surface and activate

132 the ADE cathode, they were previously polarized in 0.05 M Na<sub>2</sub>SO<sub>4</sub> at 300 mA for 60 min.  
133 The same cell without electrodes was used for the photochemical assays under UVA light.

134 Comparative photochemical and electrochemical degradations of 100 mL of 2.08 mM (50  
135 mg L<sup>-1</sup> of TOC) of oxalic (188 mg L<sup>-1</sup>) or oxamic (185 mg L<sup>-1</sup>) acid in 0.05 M Na<sub>2</sub>SO<sub>4</sub> at pH  
136 3.0 were performed. The photochemical assays with direct UVA exposition were made after  
137 addition of 0.5 mM Fe<sup>2+</sup> (UVA-Fe<sup>2+</sup>) or 0.5 mM Fe<sup>3+</sup> (UVA-Fe<sup>3+</sup>). The electrolytic methods  
138 were anodic oxidation with a BDD/SS cell (AO-BDD), the same treatment after addition of  
139 0.5 mM Fe<sup>2+</sup> (AO-BDD-Fe<sup>2+</sup>) and under UVA illumination (AO-BDD-Fe<sup>2+</sup>-UVA), and  
140 electro-Fenton with a BDD/ADE cell and 0.5 mM Fe<sup>2+</sup> (EF-BDD). For the trials with UVA  
141 irradiation, a Philips TL/6W/08 fluorescent black light blue tube placed at 7 cm above the  
142 solution was employed. The tube emitted UVA light in the wavelength region 320-420 nm  
143 with  $\lambda_{\text{max}} = 360$  nm, supplying a photoionization energy of 5 W m<sup>-2</sup> as detected with a Kipp &  
144 Zonen CUV 5 radiometer. In all experiments, the solution was kept at 35.0 °C under vigorous  
145 stirring with a magnetic bar at 800 rpm to ensure its homogenization, as well as the transport  
146 of reactants towards/from the electrodes in the electrolytic assays.

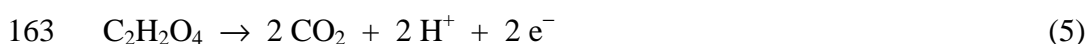
147 CV measurements were carried out with a three-electrode one-compartment cell  
148 thermostated at 25 °C. The working electrode was a 0.40 cm<sup>2</sup> BDD, the counter reference was  
149 a Pt wire and the reference electrode was a Ag|AgCl|KCl (saturated) electrode ( $E^{\circ} = 0.197$   
150 V/SHE). Cyclic voltammograms were recorded at a scan rate of 100 mV s<sup>-1</sup> under an Ar  
151 atmosphere after previous bubbling of this gas through the solution for 30 min.

#### 152 2.4. Analytical procedures

153 Before analysis, aliquots withdrawn from treated solutions were filtered with 0.45 μm  
154 PTFE filters from Whatman. Reproducible TOC values with an accuracy of ±1% were found  
155 by injecting 50 μL aliquots to the TOC analyzer. The mineralization current efficiency (MCE)  
156 for electrolyzed solutions at time  $t$  (h) was then calculated by Eq. (4) (Hamza et al., 2009):

$$157 \quad \text{MCE (\%)} = \frac{n F V_s \Delta(\text{TOC})_{\text{exp}}}{4.32 \times 10^7 m I t} \times 100 \quad (4)$$

158 where  $F$  is the Faraday constant ( $96487 \text{ C mol}^{-1}$ ),  $V_s$  is the solution volume (L),  $\Delta(\text{TOC})_{\text{exp}}$  is  
 159 the experimental TOC removal ( $\text{mg L}^{-1}$ ),  $4.32 \times 10^7$  is a conversion factor ( $3600 \text{ s h}^{-1} \times 12000$   
 160  $\text{mg mol}^{-1}$ ),  $m$  is the number of carbon atoms of each acid (2 C atoms) and  $I$  is the current (A).  
 161 The number of electrons ( $n$ ) consumed was taken as 2 for oxalic acid and 10 for oxamic acid,  
 162 assuming that their overall mineralization corresponds to reactions (5) and (6), respectively:



165 The ion-exclusion HPLC measurements were made after injection of 20  $\mu\text{L}$  aliquots into  
 166 the liquid chromatograph and circulation of 4 mM  $\text{H}_2\text{SO}_4$  at  $0.6 \text{ mL min}^{-1}$  as mobile phase.  
 167 Ionic chromatography was performed with 25  $\mu\text{L}$  aliquots using a mobile phase composed of  
 168 5.0 mM tartaric acid, 1.0 mM dipicolinic acid, 24.2 mM boric acid and 1.5 mM corona ether  
 169 at  $1.0 \text{ mL min}^{-1}$  for  $\text{NH}_4^+$  and 2.4 mM tris(hydroxymethyl)aminomethane and 2.5 mM  
 170 phthalic acid of pH 4.0 at  $1.5 \text{ mL min}^{-1}$  for  $\text{NO}_3^-$ .

### 171 3. Results and discussion

#### 172 3.1. CV behavior of oxalic and oxamic acids and their iron complexes

173 Fig. 1a shows the cyclic voltammograms obtained for the oxidation of 2.08 mM oxalic  
 174 and oxamic acids in 0.05 M  $\text{Na}_2\text{SO}_4$  on a BDD electrode at pH 3.0 and  $100 \text{ mV s}^{-1}$ . Both  
 175 compounds display an irreversible peak, with an anodic peak potential ( $E_p^{\text{a}}$ ) of 2.10 and 2.14  
 176 V for oxalic and oxamic acids, respectively, which partially overlap with that of water  
 177 discharge to  $\text{O}_2$  beginning at 2.2 V. The CV behaviour found for oxalic acid agrees with that  
 178 reported by other authors (Martínez-Huitle et al., 2004; Weiss et al., 2007; Scialdone et al.,  
 179 2008), who suggested the direct anodic oxidation of the acid at the BDD anode surface rather

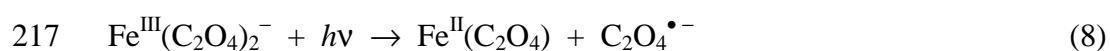
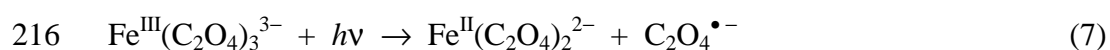
180 than its mediated reaction with BDD( $\bullet$ OH) produced from reaction (1) to be converted into  
181  $\text{CO}_2$ . This behavior can also be extended to the case of oxamic acid, which is oxidized at  
182 slightly higher potentials than oxalic acid and with a greater peak current due to the additional  
183 transformation of its  $-\text{NH}_2$  group into inorganic ions.

184 The comparative cyclic voltammograms recorded for the above acids in the presence of  
185  $0.5 \text{ mM Fe}^{2+}$  or  $0.5 \text{ mM Fe}^{3+}$  are depicted in Fig. 1b. Fe(II)- or Fe(III)-carboxylate complexes  
186 formed are oxidized at much more positive potentials than pure acids, clearly overlapping  
187 with the water discharge region. The irreversible peak for Fe(II)-oxalate complexes with  $E_p^a =$   
188  $2.31 \text{ V}$  has much higher height than that of oxalic acid (see Fig. 1a), as a result of the more  
189 complex oxidation of their electroactive species, predominantly  $\text{Fe}^{\text{II}}(\text{C}_2\text{O}_4)_2^{2-}$  (Lan et al.  
190 2010). In contrast, the dominant  $\text{Fe}^{\text{III}}(\text{C}_2\text{O}_4)_3^{3-}$  and  $\text{Fe}^{\text{III}}(\text{C}_2\text{O}_4)_2^-$  ions in the solution of Fe(III)-  
191 oxalate complexes (Balmer and Sulzberger, 1999; Kwan and Chu, 2007; Lan et al., 2010) are  
192 oxidized at so high potentials that any peak is displayed in CV. Fe(II)- and Fe(III)-oxamate  
193 complexes exhibit a similar irreversible peak, with high  $E_p^a$  of  $2.54$  and  $2.72 \text{ V}$ , respectively,  
194 suggesting that their ionic structures (not reported in literature) are analogous to those of iron-  
195 oxalate complexes, although the Fe(III)-oxamate species are more easily oxidizable. This is  
196 not surprising since oxamic like oxalic acid behaves as a bidentate ligand, coordinated with  
197 the amidic N, after ionization of one amidic H, and with the carboxylate O (Pardo et al.,  
198 2004). The fact that the iron complexes of oxalic and oxamic acids are destroyed in the water  
199 discharge zone indicates that they react predominantly with BDD( $\bullet$ OH) at the anode surface.

### 200 *3.2. Photochemical degradation of oxalic and oxamic acids and their iron complexes*

201 A series of trials was made to assess the degradation effect of the  $6 \text{ W UVA}$  light on  $100$   
202  $\text{mL}$  of the  $2.08 \text{ mM}$  acid solutions in the absence and presence of  $0.5 \text{ mM Fe}^{2+}$  or  $0.5 \text{ mM}$   
203  $\text{Fe}^{3+}$ . The evolution of each compound was monitored by ion-exclusion chromatography,  
204 which displayed a well-defined adsorption peak at retention time of  $6.8 \text{ min}$  for oxalic acid

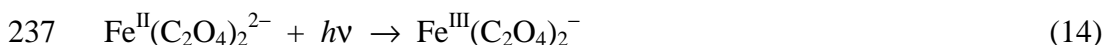
205 and 9.4 min for oxamic acid. Fig. 2a and 2b show that both acids are very stable under UVA  
 206 irradiation, as expected if they are not directly photolyzed. In contrast, their iron complexes  
 207 are photodegraded at different rate depending on the acid and iron ion tested. The fastest  
 208 removal was found for the UVA-Fe<sup>3+</sup> treatment of oxalic acid, which disappears in about 150  
 209 min. Overall destruction of this acid is also feasible using UVA-Fe<sup>2+</sup>, although a longer time  
 210 close to 360 min is required. The kinetic analysis of these experiments showed good linear  
 211 correlations for a pseudo first-order reaction. The pseudo first-order rate constant ( $k_{\text{oxalic}}$ ) thus  
 212 determined, along the corresponding square of regression coefficient, are collected in Table 1.  
 213 The quick photodegradation of Fe(III)-oxalate complexes can be accounted for by the high  
 214 photoactivity of their dominant ionic species by reactions (7) and (8) (Faust and Zepp, 1993;  
 215 Balmer and Sulzberger, 1999; Jeong and Yoon, 2005):



218 These reactions are photoredox processes with a ligand-to-metal charge transfer leading to the  
 219 homolytic break of a Fe(III)-O coordination bond of the bidentate oxalate ligand (Šima and  
 220 Makáňová, 1997). The anion radical  $\text{C}_2\text{O}_4^{\bullet-}$  released yields  $\text{CO}_2$  and the anion radical  $\text{CO}_2^{\bullet-}$   
 221 by reaction (9), which then reacts with dissolved  $\text{O}_2$  to produce the ion superoxide ( $\text{O}_2^{\bullet-}$ ) from  
 222 reaction (10). This specie originates a cascade of other ROS like hydroperoxide radical  
 223 ( $\text{HO}_2^{\bullet}$ ) from reaction (11) and  $\text{H}_2\text{O}_2$  from reaction (12).  $\text{H}_2\text{O}_2$  can further oxidize the Fe(II) to  
 224 Fe(III) complexes, as exemplified for  $\text{Fe}^{\text{II}}(\text{C}_2\text{O}_4)_2^{2-}$  in reaction (13), at a rate about 1000 times  
 225 higher than that of Fenton's reaction (3) (Faust and Zepp, 1993), thus closing the  
 226 Fe(III)/Fe(II) catalytic loop. The large production of  $\bullet\text{OH}$  from the reaction (13), which does  
 227 not attack the iron-oxalate complexes, has been well proven in photoassisted ferrioxalate  
 228 systems (Jeong and Yoon, 2005; Rodríguez et al., 2007; Monteagudo et al., 2008).



234 The slow decay of oxalic acid in the UVA-Fe<sup>2+</sup> system can then be related to the much  
 235 lower photoactivity of Fe(II) complexes to be converted into Fe(III) ones, as exemplified by  
 236 reaction (14) (Faust and Zepp, 1993; Kwan and Chu, 2007):



238 Once the Fe(III)-oxalate complexes are formed, a photodegradation path similar to that  
 239 described above for the UVA-Fe<sup>3+</sup> treatment takes place, although the large preponderance of  
 240 Fe(II)-oxalate complexes at the beginning of the process makes it slower.

241 The aforementioned experiments for oxalic acid were performed with 7.6 mg L<sup>-1</sup> of  
 242 dissolved O<sub>2</sub>. To clarify the generation of ROS via reactions (10)-(12), the same trials were  
 243 repeated with 28.0 mg O<sub>2</sub> L<sup>-1</sup> in solution under O<sub>2</sub> bubbling at 0.5 L min<sup>-1</sup>. Results of Table 1  
 244 confirm the increase in *k*<sub>oxalic</sub> in both systems, much more for UVA-Fe<sup>2+</sup> (1.77-fold) than for  
 245 UVA-Fe<sup>3+</sup> (1.06-fold). The excess of H<sub>2</sub>O<sub>2</sub> formed under O<sub>2</sub> bubbling strongly accelerates the  
 246 oxidation of Fe<sup>II</sup>(C<sub>2</sub>O<sub>4</sub>)<sub>2</sub><sup>2-</sup> by reaction (13) in UVA-Fe<sup>2+</sup>, while this reaction is only slightly  
 247 enhanced in UVA-Fe<sup>3+</sup> due to the much lower concentration of Fe(II) species.

248 Fig. 2b evidences that the very low photoactivity of Fe(II)- and Fe(III)-oxamate  
 249 complexes only allows a 57% and 77% destruction of the acid after 360 min of UVA-Fe<sup>2+</sup> and  
 250 UVA-Fe<sup>3+</sup> treatments, respectively. This is also reflected in the low pseudo first-order rate  
 251 constant (*k*<sub>oxamic</sub>) values obtained (see Table 1). As can be seen in Fig. 3, a larger percentage  
 252 of its initial N is lost as NH<sub>4</sub><sup>+</sup> (43% for UVA-Fe<sup>2+</sup> and 65% for UVA-Fe<sup>3+</sup>) at the end of these

253 trials, although the oxidation to  $\text{NO}_3^-$  is significant in both cases (9% of initial N for UVA-  
254  $\text{Fe}^{2+}$  and 12% of initial N for UVA- $\text{Fe}^{3+}$ ). Note that for the UVA- $\text{Fe}^{2+}$  system, about 5% of  
255 initial N is released as volatile compounds, probably  $\text{NO}_x$  species.

### 256 3.3. Mineralization of oxalic acid by EAOPs

257 Comparative degradations of 100 mL of 2.08 mM oxalic acid by different EAOPs were  
258 made at  $33.3 \text{ mA cm}^{-2}$ . Fig. 2a shows that this acid is completely removed at 300 min of the  
259 AO-BDD treatment, since it is transformed into  $\text{CO}_2$  by direct oxidation at the anode, as  
260 stated above. When 0.5 mM  $\text{Fe}^{2+}$  is added to the solution, a strong inhibition of oxalic acid  
261 decay occurs during the AO-BDD- $\text{Fe}^{2+}$  process, only being reduced by 72% after 360 min of  
262 electrolysis. A similar tendency can be observed in Fig. 2a for the EF-BDD system, where the  
263 large generation of  $\text{H}_2\text{O}_2$  from the ADE cathode favors the rapid conversion of Fe(II)- into  
264 Fe(III)-oxalate complexes, e.g. via reaction (13). This suggests that in AO-BDD- $\text{Fe}^{2+}$ , the  
265 initial Fe(II)-oxalate complexes are quickly oxidized to Fe(III)-oxalate species by BDD( $\bullet\text{OH}$ )  
266 at the anode surface. This oxidation is also feasible with  $\text{H}_2\text{O}_2$  since it is produced in low  
267 amounts from dimerization of BDD( $\bullet\text{OH}$ ) by reaction (15) (Guinea et al., 2009):



269 The slow destruction of Fe(III)-oxalate complexes with BDD( $\bullet\text{OH}$ ), as confirmed by CV (see  
270 Fig. 1b), then explains the similar and slow abatement of the acid in AO-BDD- $\text{Fe}^{2+}$  and EF-  
271 BDD, without oxidation by  $\bullet\text{OH}$  formed from Fenton's reaction (3). From these results, the  
272 effect of UVA illumination was studied for the AO-BDD- $\text{Fe}^{2+}$ -UVA treatment. Fig. 2a shows  
273 that this EAOP leads to total destruction of the acid in only 90 min, as expected from the  
274 rapid photolysis of Fe(III)-oxalate complexes. Since a steady concentration of  $13 \text{ mg O}_2 \text{ L}^{-1}$   
275 was reached in this trial, significant amounts of  $\text{H}_2\text{O}_2$  are formed from reaction (12), which  
276 contribute to the oxidation of Fe(II)- to Fe(III)-oxalate complexes.

277 The  $k_{\text{oxalic}}$  value obtained for the above EAOPs is listed in Table 1. It increased 1.40-fold  
278 for the most potent AO-BDD-Fe<sup>2+</sup>-UVA system compared with UV-Fe<sup>3+</sup>, as expected if the  
279 photoactive Fe(III)-oxalate species are more quickly regenerated, involving its oxidation with  
280 H<sub>2</sub>O<sub>2</sub> from reaction (13) and with BDD(<sup>•</sup>OH) at the anode surface.

281 TOC was always removed in a similar way to oxalic acid due to the insignificant  
282 formation of by-products. For example, after 360 min of AO-BDD-Fe<sup>2+</sup> and EF-BDD, TOC  
283 was reduced to 13 mg L<sup>-1</sup>, corresponding to 49 mg L<sup>-1</sup> oxalic acid in good agreement with 52  
284 mg L<sup>-1</sup> found for the final electrolyzed solutions (see Fig. 2a). Total mineralization was  
285 achieved after about 300 min of AO-BDD and close to 90 min of AO-BDD-Fe<sup>2+</sup>-UVA, times  
286 similar to those required for the total removal of oxalic acid, as shown in Fig. 2a. The  
287 efficiency calculated from Eq. (4) decreased with electrolysis time by the gradual drop in  
288 oxalic acid content. For example, the MCE value decayed from 7.2% or 12.5% at 10 min to  
289 1.6% or 6.7% at the end of the AO-BDD or AO-BDD-Fe<sup>2+</sup>-UVA treatment.

290 From the above results, the reaction sequence of Fig. 4 is proposed for oxalic acid  
291 mineralization by AO-BDD-Fe<sup>2+</sup>-UVA. It is initiated by the oxidation of Fe<sup>II</sup>(C<sub>2</sub>O<sub>4</sub>)<sub>2</sub><sup>2-</sup> with  
292 BDD(<sup>•</sup>OH) to yield Fe<sup>III</sup>(C<sub>2</sub>O<sub>4</sub>)<sub>2</sub><sup>-</sup>, in equilibrium with Fe<sup>III</sup>(C<sub>2</sub>O<sub>4</sub>)<sub>3</sub><sup>3-</sup>. These ionic species are  
293 quickly photolyzed regenerating Fe<sup>II</sup>(C<sub>2</sub>O<sub>4</sub>) and Fe<sup>II</sup>(C<sub>2</sub>O<sub>4</sub>)<sub>2</sub><sup>2-</sup>, respectively, with the loss of  
294 CO<sub>2</sub> and CO<sub>2</sub><sup>•-</sup>. Further reaction of CO<sub>2</sub><sup>•-</sup> with O<sub>2</sub> originates CO<sub>2</sub> and ROS. The catalytic  
295 loop between Fe(II)- and Fe(III)-oxalate complexes is then propagated by the continuous  
296 oxidation of Fe<sup>II</sup>(C<sub>2</sub>O<sub>4</sub>)<sub>2</sub><sup>2-</sup> with BDD(<sup>•</sup>OH) and ROS (primordially H<sub>2</sub>O<sub>2</sub>). All ionic species  
297 can also be oxidized to CO<sub>2</sub> at the BDD anode, although reactions with BDD(<sup>•</sup>OH) are much  
298 slower than the photodegradation of Fe(III) species with UVA light. A slow oxidation of  
299 oxalic acid, in equilibrium with the above complexes, at the anode is also feasible.

300 *3.4. Mineralization of oxamic acid by EAOPs*

301 The degradation of 2.08 mM oxamic acid solutions by the same EAOPs always followed  
302 a pseudo first-order abatement. Fig. 2b evidences that AO-BDD-Fe<sup>2+</sup> and EF-BDD processes  
303 yield the same decay rate for this acid, as expected if its Fe(II) complexes are oxidized by  
304 BDD(<sup>•</sup>OH) with insignificant participation of <sup>•</sup>OH in the bulk. Both treatments are more  
305 potent than AO-BDD because of the most effective destruction of Fe(III)-oxamate complexes  
306 by BDD(<sup>•</sup>OH) than that of oxamic acid by direct charge transfer. Comparison of Fig. 2a and  
307 2b evidences that AO-BDD-Fe<sup>2+</sup> and EF-BDD methods are more effective for the abatement  
308 of oxamic than oxalic acid, in agreement with the higher oxidation ability of Fe(III)-oxamate  
309 species at BDD (see Fig. 1b). Fig. 2b also shows that oxamic acid disappears in 270 min for  
310 AO-BDD-Fe<sup>2+</sup>-UVA. Since  $k_{\text{oxamic}}$  for this method is 2.56 times higher than for UV-Fe<sup>3+</sup> (see  
311 Table 1), one can infer that Fe(III)-oxamate species are rapidly formed from the oxidation of  
312 Fe(II)-oxamate ones with BDD(<sup>•</sup>OH) and generated H<sub>2</sub>O<sub>2</sub> to be photolyzed by UVA light  
313 regenerating the Fe(II) species with loss of CO<sub>2</sub> and inorganic N products. Results of Table 1  
314 indicate that  $k_{\text{oxalic}} > k_{\text{oxamic}}$  for AO-BDD and AO-BDD-Fe<sup>2+</sup>-UVA, while  $k_{\text{oxalic}} < k_{\text{oxamic}}$  for  
315 AO-BDD-Fe<sup>2+</sup> and EF-BDD. That means that oxamic acid is more recalcitrant than oxalic  
316 acid only in the two former methods, but not in the two latter. For the EAOPs tested, TOC  
317 was removed similarly to oxamic acid, indicating the formation of insignificant amounts of  
318 organic by-products during all mineralization processes. In addition, the progressive loss in  
319 oxidizable organic matter caused a continuous fall in MCE.

320 Fig. 3 illustrates the predominance of N lost as NH<sub>4</sub><sup>+</sup> ion at the end of all EAOPs tested to  
321 mineralize the 2.08 mM oxalic acid solution at 33.3 mA cm<sup>-2</sup>. The larger proportion of N lost  
322 as NO<sub>3</sub><sup>-</sup> ion is found for AO-BDD, indicating that NH<sub>4</sub><sup>+</sup> ion is preferentially formed during  
323 the oxidation of Fe(III)-oxamate species than oxamic acid. TN analysis of final electrolyzed  
324 solutions confirmed the release of N as NO<sub>x</sub> species. For AO-BDD-Fe<sup>2+</sup>-UVA, for example,  
325 the initial 29.6 mg L<sup>-1</sup> of N were reduced to 23.1 mg L<sup>-1</sup> in 270 min, i.e. when all oxamic acid

326 is mineralized, corresponding to a loss of 21.9% of N as NO<sub>x</sub> species, a value close to 21.8%  
327 determined from the N obtained for NH<sub>4</sub><sup>+</sup> (64%) and NO<sub>3</sub><sup>-</sup> (14.2%), as depicted in Fig. 3.

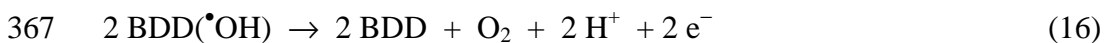
### 328 3.5. Mineralization of mixtures of oxalic and oxamic acid by EAOPs

329 Since a mixture of oxalic and oxamic acid is obtained as ultimate by-product of the  
330 degradation of *N*-aromatics by EAOPs (Sirés et al., 2006; Hammami et al., 2008; Hamza et  
331 al., 2009), the possible influence of the relative proportion of both acids on their removal rate  
332 was investigated. To do this, 8%, 25% and 43% of oxamic acid was added to the 2.08 mM  
333 oxalic acid solution to be treated by AO-BDD, AO-BDD-Fe<sup>2+</sup> and AO-BDD-Fe<sup>2+</sup>-UVA at  
334 33.3 mA cm<sup>-2</sup>, after adding 0.5 mM Fe<sup>2+</sup> in the two latter methods. The  $k_{\text{oxamic}}$  and  $k_{\text{oxalic}}$   
335 values determined simultaneously for these experiments are summarized in Table 2.

336 For AO-BDD, similar  $k_{\text{oxamic}} \sim 1.1 \times 10^{-4} \text{ s}^{-1}$  and  $k_{\text{oxalic}} \sim 1.5 \times 10^{-4} \text{ s}^{-1}$  to that of pure  
337 solutions (see Table 1) are found, evidencing that both acids are independently oxidized at the  
338 BDD anode via direct charge transfer. In contrast, the competition between Fe(III)-oxamate  
339 and Fe(III)-oxalate complexes causes a change in the removal rate of acids in the EAOPs with  
340 Fe<sup>2+</sup>. Thus, for AO-BDD-Fe<sup>2+</sup>,  $k_{\text{oxalic}}$  gradually decays with decreasing the percentage of  
341 oxamic acid, while  $k_{\text{oxamic}} \sim 1.3 \times 10^{-4} \text{ s}^{-1}$  is similar to  $1.2 \times 10^{-4} \text{ s}^{-1}$  for pure iron-oxamate  
342 complexes (see Table 1). This deceleration of oxalic acid removal is due to the progressive  
343 formation of a larger proportion of Fe(III)-oxalate complexes that are more difficultly  
344 oxidized with BDD(<sup>•</sup>OH). The much faster destruction of Fe(III)-oxamate species with this  
345 radical explains the slight change in  $k_{\text{oxamic}}$  in all mixtures. The smaller amount of Fe(III)-  
346 oxamate species formed and the rise in Fe(III)-oxalate ones with decreasing the percentage of  
347 oxamic acid are also reflected in AO-BDD-Fe<sup>2+</sup>-UVA, where the low photoactivity of the  
348 former accounts for the drop in  $k_{\text{oxamic}}$ , whereas the much greater photoactivity of the latter  
349 justifies the slight increase in  $k_{\text{oxalic}}$ . A slower removal of oxamic acid is then expected as its  
350 content decreases, without significant effect on oxalic acid decay.

351 3.6. Effect of current density and  $Fe^{2+}$  content on the mineralization of oxamic acid by AO-  
352 BDD- $Fe^{2+}$ -UVA

353 The abatement of TOC and oxamic acid content between 16.6 and 100 mA cm<sup>-2</sup> for the  
354 most potent AO-BDD- $Fe^{2+}$ -UVA process is presented in Fig. 5a and 5b, respectively. The rise  
355 in current density accelerates the decay of both parameters, enhancing the oxidation power of  
356 the process. The time required for overall mineralization (see Fig. 5a) is slightly longer than  
357 that needed for total destruction of the acid (see Fig. 5b), as expected if very low amounts of  
358 more recalcitrant by-products are formed. A progressive loss in MCE as current density  
359 increases can be observed in the inset panel of Fig. 5a, whereas the opposite trend is found for  
360  $k_{oxamic}$  in the inset panel of Fig. 5b, which gradually increases from  $1.48 \times 10^{-4} \text{ s}^{-1}$  ( $R^2 = 0.999$ )  
361 for 16.6 mA cm<sup>-2</sup> to  $3.15 \times 10^{-4} \text{ s}^{-1}$  ( $R^2 = 0.996$ ) for 100 mA cm<sup>-2</sup>. This behavior agrees with the  
362 expected production of more amounts of oxidant BDD( $\bullet$ OH) from reaction (1) at greater  
363 current density (Brillas et al., 2009; Panizza and Cerisola, 2009), accelerating the oxidation of  
364 Fe(II) into Fe(III) complexes to be more quickly photolyzed by UVA light. The loss in  
365 efficiency evidences that the excess of generated BDD( $\bullet$ OH) is mainly wasted by oxidation to  
366 O<sub>2</sub> via reaction (16) (Marselli et al., 2003; Panizza and Cerisola, 2009):



368 The evolution of  $NH_4^+$  and  $NO_3^-$  ions detected during 360 min in the above experiments is  
369 shown in Fig. 6a and 6b, respectively.  $NH_4^+$  ion is continuously accumulated up to 33.3 mA  
370 cm<sup>-2</sup>, but it undergoes a gradual drop as electrolysis time is prolonged at current densities  $\geq$   
371 66.6 mA cm<sup>-2</sup>. The fast removal of  $NH_4^+$  ion at 100 mA cm<sup>-2</sup> is accompanied by a large  $NO_3^-$   
372 accumulation, while much lower contents of this ion are found at lower current densities.  
373 Increasing percentages of N lost as  $NO_x$  species of 15.3%, 21.8%, 44.0% and 55.5% were  
374 thus determined for 16.6, 33.3, 66.6 and 100 mA cm<sup>-2</sup>, also confirmed from TN analysis of

375 final electrolyzed solutions. These findings suggests that high current densities accelerate the  
376 parasite oxidation of  $\text{NH}_4^+$  to  $\text{NO}_3^-$  ion with the greater amounts of BDD( $\bullet\text{OH}$ ) produced,  
377 increasing the loss of  $\text{NO}_x$  species. This suggestion was corroborated by electrolyzing a  
378  $(\text{NH}_4)_2\text{SO}_4$  solution with  $20 \text{ mg L}^{-1}$  of N under similar conditions. For  $100 \text{ mA cm}^{-2}$ ,  $\text{NH}_4^+$  ion  
379 was totally removed in 270 min generating  $4.6 \text{ mg L}^{-1}$  of N as  $\text{NO}_3^-$  ion and releasing 78% of  
380 N as  $\text{NO}_x$  species. In contrast, after 360 min of electrolysis at  $33.3 \text{ mA cm}^{-2}$ ,  $11.3 \text{ mg L}^{-1}$  of N  
381 as  $\text{NH}_4^+$  ion and  $1.2 \text{ mg L}^{-1}$  of N as  $\text{NO}_3^-$  ion were found, with loss of 37% of N as  $\text{NO}_x$   
382 species. Note that  $\text{NH}_4^+$  is converted into  $\text{NO}_3^-$  in larger extent in the treatment of  $(\text{NH}_4)_2\text{SO}_4$   
383 than oxamic acid, probably because  $\text{NH}_4^+$  ion is gradually released to the medium in the latter  
384 case and its oxidation at the BDD anode competes with that of iron-oxamate complexes.

385 Fig. 7a evidences that oxamic acid removal is inhibited with increasing  $\text{Fe}^{2+}$  content. This  
386 trend can be related to a gradual decay in rate of the reaction between Fe(II)-oxamate species  
387 and BDD( $\bullet\text{OH}$ ), decelerating its conversion into photoactive Fe(III) complexes, due to the  
388 competition of the oxidation of larger amounts of free  $\text{Fe}^{2+}$  to  $\text{Fe}^{3+}$  ion at the anode (Sirés et  
389 al., 2007). The reduction of  $\text{Fe}^{3+}$  ion at the SS cathode regenerates the  $\text{Fe}^{2+}$  ion and maintains  
390 the equilibrium between both ions in solution (Brillas et al., 2009). The loss of oxidation  
391 ability of the system is also reflected in Fig. 7b, where higher  $\text{Fe}^{2+}$  content causes a gradual  
392 decay in the percentage of N lost as  $\text{NO}_3^-$  ion and a larger proportion of N lost as  $\text{NH}_4^+$  ion,  
393 with a similar percentage of N lost as  $\text{NO}_x$  species. The presence of small amounts of  $\text{Fe}^{2+}$  in  
394 solution then minimizes the undesired oxidation of  $\text{Fe}^{2+}$  at the anode, favouring the rapid  
395 conversion of Fe(II)-oxamate complexes into photoactive Fe(III)-oxamate species.

#### 396 4. Conclusions

397 Oxalic and oxamic acids were efficiently mineralized by AO-BDD- $\text{Fe}^{2+}$ -UVA, as a result  
398 of the high photoactivity of their Fe(III) complexes that are continuously regenerated by

399 oxidation of their Fe(II) complexes with BDD( $\bullet$ OH) formed at the anode surface and H<sub>2</sub>O<sub>2</sub>  
400 generated from O<sub>2</sub> reduction or BDD( $\bullet$ OH) dimerization. In this method, oxamic acid was  
401 more recalcitrant by the lower photoactivity of its Fe(III) complexes, releasing a larger  
402 proportion of NH<sub>4</sub><sup>+</sup> than NO<sub>3</sub><sup>-</sup> ion. The loss of volatile NO<sub>x</sub> species was confirmed from TN  
403 analysis of the final electrolyzed solutions. Each acid underwent a similar decay in AO-BDD-  
404 Fe<sup>2+</sup> and EF-BDD since its iron complexes were not attacked with  $\bullet$ OH in the bulk. AO-BDD  
405 also allowed the total conversion of oxalic acid into CO<sub>2</sub> by direct charge transfer at the  
406 anode. This process explained the slower destruction of oxamic acid by this method. In  
407 contrast, oxamic acid was less recalcitrant in AO-BDD-Fe<sup>2+</sup> and EF-BDD, since Fe(III)-  
408 oxamate complexes were oxidized more quickly with BDD( $\bullet$ OH) than Fe(III)-oxalate ones.  
409 TOC always decayed similarly to the corresponding acid, indicating a insignificant formation  
410 of by-products. While both acids when mixed were independently oxidized at the anode in  
411 AO-BDD, the proportion of their Fe(III) complexes and their ability to be oxidized and/or  
412 photolyzed affected their degradation rate in the EAOPs with Fe<sup>2+</sup>. For the most potent AO-  
413 BDD-Fe<sup>2+</sup>-UVA, a lower oxamic acid content decelerated its degradation, without significant  
414 effect on oxalic acid decay. Greater current density enhanced the oxidation power of this  
415 method since oxamic acid removal was accelerated, but losing efficiency. High Fe<sup>2+</sup> contents  
416 inhibited the oxidation of Fe(II)-oxamate complexes by the competitive oxidation of free Fe<sup>2+</sup>  
417 to Fe<sup>3+</sup>. Low current densities and Fe<sup>2+</sup> contents are then preferable for the more efficient  
418 removal of these acids in AO-BDD-Fe<sup>2+</sup>-UVA.

## 419 **Acknowledgement**

420 The authors acknowledge financial support from MICINN (Ministerio de Ciencia e  
421 Innovación, Spain) under the project CTQ2010-16164/BQU, cofinanced with FEDER funds.  
422 S. G.-S. thanks the grant awarded from MEC (Ministerio de Educación y Ciencia, Spain).

423 **References**

- 424 Andreozzi, R., Caprio, V., Insola, A., Marotta, R., 1999. Advanced oxidation processes  
425 (AOP) for water purification and recovery. *Catal. Today* 53 (1), 51-59.
- 426 Balci, B., Oturan, N., Cherrier, R., Oturan, M.A. 2009. Degradation of atrazine in aqueous  
427 medium by electrocatalytically generated hydroxyl radicals. A kinetic and mechanistic  
428 study. *Water Res.* 43 (7), 1924-1934.
- 429 Balmer, M.E., Sulzberger, B., 1999. Atrazine degradation in irradiated iron/oxalate systems:  
430 Effects of pH and oxalate. *Environ. Sci. Technol.* 33 (14), 2418-2424.
- 431 Brillas, E., Baños, M.A., Camps, S., Arias, C., Cabot, P.L., Garrido, J.A., Rodríguez, R.M.,  
432 2004. Catalytic effect of  $\text{Fe}^{2+}$ ,  $\text{Cu}^{2+}$  and UVA light on the electrochemical degradation of  
433 nitrobenzene using an oxygen-diffusion cathode. *New J. Chem.* 28 (2), 314-322.
- 434 Brillas, E., Sirés, I., Oturan, M.A., 2009. Electro-Fenton process and related electrochemical  
435 technologies based on Fenton's reaction chemistry. *Chem. Rev.* 109 (12), 6570-6631.
- 436 Brillas, E., Garcia-Segura, S., Skoumal, M., Arias, C., 2010. Electrochemical incineration of  
437 diclofenac in neutral aqueous medium by anodic oxidation using Pt and boron-doped  
438 diamond anodes. *Chemosphere* 79 (6), 605-612.
- 439 Cañizares, P., García-Gómez, J., Lobato, J., Rodrigo, M.A., 2003. Electrochemical oxidation  
440 of aqueous carboxylic acid wastes using diamond thin-film electrodes. *Ind. Eng. Chem.*  
441 *Res.* 42 (5), 956-962.
- 442 Cañizares, P., Beteta, A., Saez, C., Rodríguez, L., Rodrigo, M.A., 2008. Use of  
443 electrochemical technology to increase the quality of the effluents of bio-oxidation  
444 processes. A case studied. *Chemosphere* 72 (7), 1080-1085.
- 445 Diagne, M., Oturan, N., Mehmet A.Oturan, M.A., 2007. Removal of methyl parathion from  
446 water by electrochemically generated Fenton's reagent. *Chemosphere* 66 (5), 841-848.

447 Faria, P.C.C., Órfão, J.J.M., Pereira, M.F.R., 2008. Activated carbon catalytic ozonation of  
448 oxamic and oxalic acids. *Appl. Catal. B: Environ.* 79 (3), 237–243.

449 Faust, B.C., Zepp, R.G., 1993. Photochemistry of aqueous iron(III)-polycarboxylate  
450 complexes: roles in the chemistry of atmospheric and surface waters. *Env. Sci. Technol.*  
451 27 (12), 2517-2522.

452 Gandini, D., Mahé, E., Michaud, P.A., Haenni, W., Perret, A., Comninellis, Ch., 2000.  
453 Oxidation of carboxylic acids at boron-doped diamond electrodes for wastewater  
454 treatment. *J. Appl. Electrochem.* 30 (12), 1345-1350.

455 Guinea E., Centellas, F., Garrido, J.A., Rodríguez, R.M., Arias, C., Cabot, P.L., Brillas, E.,  
456 2009. Solar photoassisted anodic oxidation of carboxylic acids in presence of  $\text{Fe}^{3+}$  using a  
457 boron-doped diamond electrode. *Appl. Catal. B: Environ.* 89 (3-4), 459-468.

458 Hammami, S., Bellakhal, N., Oturan, N., Oturan, M.A., Dachraoui, M., 2008. Degradation of  
459 Acid Orange 7 by electrochemically generated  $\cdot\text{OH}$  radicals in acidic aqueous medium  
460 using a boron-doped diamond or platinum anode. A mechanistic study. *Chemosphere* 73  
461 (5), 678-684.

462 Hamza, M., Abdelhedi, R., Brillas, E., Sirés, I., 2009. Comparative electrochemical  
463 degradation of the triphenylmethane dye metil violet with boron-doped diamond and Pt  
464 anodes. *J. Electroanal. Chem.* 627 (1-2), 41-50.

465 Jeong, J., Yoon, J., 2005. pH effect on OH radical production in photo/ferrioxalate system.  
466 *Water Res.* 39 (13), 2893-2900.

467 Kwan, C.Y., Chu, W., 2007. The role of organic ligands in ferrous-induced photochemical  
468 degradation of 2,4-dichlorophenoxyacetic acid. *Chemosphere* 67 (8), 1601-1611.

469 Lan, Q., Li, F.B., Sun, C.X., Liu, C.S., Li, X.Z., 2010. Heterogeneous photodegradation of  
470 pentachlorophenol and iron cycling with goethite, hematite and oxalate under UVA  
471 illumination. *J. Hazard. Mater.* 174 (1-3), 64-70.

472 Martínez-Huitle, C.A., Ferro, S., De Battisti, A., 2004. Electrochemical incineration of oxalic  
473 acid: Role of electrode material. *Electrochim. Acta* 49 (22-23), 4027-4034.

474 Marselli, B., García-Gómez, J., Michaud, P.A., Rodrigo, M.A., Cominellis, Ch., 2003.  
475 Electrogeneration of hydroxyl radicals on boron-doped diamond electrodes. *J.*  
476 *Electrochem. Soc.* 150 (3), D79-D83.

477 Monteagudo, J.M., Durán, A., López-Almodóvar, C., 2008. Homogeneous ferrioxalate-assisted  
478 solar photo-Fenton degradation of Orange II aqueous solutions. *Appl. Catal. B: Environ.*  
479 83 (1-2), 46-55.

480 Oturan, M.A., Pimentel, M., Oturan, N., Sirés, I., 2008. Reaction sequence for the  
481 mineralization of the short-chain carboxylic acids usually formed upon cleavage of  
482 aromatics during electrochemical Fenton treatment. *Electrochim. Acta* 54(2), 173-182.

483 Özcan, A., Şahin, Y., Koparal, A.S., Oturan, M.A., 2008. Protham mineralization in aqueous  
484 medium by anodic oxidation using boron-doped diamond anode. Experimental  
485 parameters' influence on degradation kinetics and mineralization efficiency. *Water Res.*  
486 42 (12), 2889-2898.

487 Panizza, M., Cerisola, G., 2009. Direct and mediated anodic oxidation of organic pollutants.  
488 *Chem. Rev.* 109 (12), 6541-6569.

489 Pardo, E., Lloret, F., Carrasco, R., M. Muñoz, C., Temporal-Sánchez, T., Ruiz-García R.,  
490 2004. Chemistry and reactivity of dinuclear iron oxamate complexes: alkane oxidation  
491 with hydrogen peroxide catalysed by an oxo-bridged diiron(III) complex with amide and  
492 carboxylate ligation. *Inorg. Chim. Acta* 357 (9), 2713-2720.

493 Pera-Titus, M., García-Molina, V., Baños, M.A., Giménez, J., Esplugas, S., 2004.  
494 Degradation of chlorophenols by means of advanced oxidation processes: a general  
495 review. *Appl. Catal. B: Environ.* 47 (4), 219-256.

496 Rodríguez, E., Mimbbrero, M., Masa, F.J., Beltrán, F.J., 2007. Homogeneous iron-catalyzed  
497 photochemical degradation of muconic acid in water. *Water Res.* 41 (6), 1325-1333.

498 Ruiz, E.J., Arias, C., Brillas, E., Hernández-Ramírez, A., Peralta-Hernández, J.M., 2011.  
499 Mineralization of Acid Yellow 36 azo dye by electro-Fenton and solar photoelectro-  
500 Fenton processes with a boron-doped diamond anode. *Chemosphere* 82 (4), 495-501.

501 Scialdone, O., Galia, A., Guarisco, C., Randazzo, S., Filardo, G., 2008. Electrochemical  
502 incineration of oxalic acid at boron doped diamond anodes: Role of operative parameters.  
503 *Electrochim. Acta* 53 (5), 2095-2108.

504 Serra, A., Domènech, X., Arias, C., Brillas, E., Peral, J., 2009. Oxidation of  $\alpha$ -  
505 methylphenylglycine under Fenton and electro-Fenton conditions in the dark and in the  
506 presence of solar light. *Appl. Catal. B: Environ.* 89 (1-2), 12-21.

507 Šima, J., Makáňová, J., 1997. Photochemistry of iron(III) complexes. *Coord. Chem. Rev.* 160,  
508 161-189.

509 Sirés, I., Garrido, J.A., Rodríguez, R.M., Cabot, P.L., Centellas, F., Arias, C., Brillas, E.,  
510 2006. Electrochemical degradation of paracetamol from water by catalytic action of  $\text{Fe}^{2+}$ ,  
511  $\text{Cu}^{2+}$ , and UVA light on electrogenerated hydrogen peroxide. *J. Electrochem. Soc.* 153  
512 (1), D1-D9.

513 Sirés, I., Centellas, F., Garrido, J.A., Rodríguez, R.M., Arias, C., Cabot, P.L., Brillas, E.,  
514 2007. Mineralization of clofibric acid by electrochemical advanced oxidation processes  
515 using a boron-doped diamond anode and  $\text{Fe}^{2+}$  and UVA light as catalysts. *Appl. Catal. B:*  
516 *Environ.* 72 (3-4), 373-381.

517 Sirés, I., Brillas, E., Cerisola, G., Panizza, M., 2008. Comparative depollution of mecoprop  
518 aqueous solutions by electrochemical incineration using BDD and  $\text{PbO}_2$  as high oxidation  
519 power anodes. *J. Electroanal. Chem.* 613 (2), 151-159.

520 Sun, Y., Pignatello, J.J., 1993. Photochemical-reactions involved in the total mineralization of  
521 2,4-D by  $\text{Fe}^{3+}/\text{H}_2\text{O}_2/\text{UV}$ . *Environ. Sci. Technol.* 27 (2), 304-310.

522 Vandini, T.A., Rao, T.N., Fujishima, A., Einaga, Y., 2006. Electrochemical oxidation of  
523 oxalic acid at highly boron-doped diamond electrodes. *Anal. Chem.* 78 (10), 3467-3471.

524 Weiss, E., Groenen-Serrano, K., Savall, A. Comninellis, Ch., 2007. A kinetic study of the  
525 electrochemical oxidation of maleic acid on boron doped diamond. *J. Electroanal. Chem.*  
526 37 (1), 41-47.

527 Zuo, Y., Hoigné, J., 1992. Formation of hydrogen peroxide and depletion of oxalic acid in  
528 atmospheric water by photolysis of iron(III)-oxalato complexes. *Environ. Sci. Technol.*  
529 26 (5), 1014-1022.

530 Zuo, Y., Hoigné, J., 1994. Photochemical decomposition of oxalic, glyoxalic and pyruvic acid  
531 catalysed by iron in atmospheric waters. *Atmos. Environ.* 28 (7), 1231-1239.

532

533 **Figure Captions**

534 **Fig. 1.** Cyclic voltammograms recorded for the oxidation of (a) 2.08 mM oxalic and oxamic  
535 acids and (b) their solutions with 0.5 mM Fe<sup>2+</sup> or 0.5 mM Fe<sup>3+</sup> in 0.05 M Na<sub>2</sub>SO<sub>4</sub> of pH 3.0  
536 on a 0.40 cm<sup>2</sup> boron-doped diamond (BDD) anode. Initial and final potentials 1.0 V, reversal  
537 potential: (a) 2.3 V and (b) 3.3 V. Scan rate 100 mV s<sup>-1</sup>. Temperature 25 °C.

538 **Fig. 2.** Decay of the concentration of (a) oxalic and (b) oxamic acids from 100 mL of 2.08  
539 mM of each carboxylic acid in 0.05 M Na<sub>2</sub>SO<sub>4</sub> at pH 3.0 and 35 °C. Method: (●) 6 W UVA  
540 irradiation (UVA), (■) 0.5 mM Fe<sup>2+</sup> solution and UVA light (UVA-Fe<sup>2+</sup>), (◆) 0.5 mM Fe<sup>3+</sup>  
541 solution and UVA light (UVA-Fe<sup>3+</sup>), (□) AO in BDD/stainless steel (SS) cell (AO-BDD), (△)  
542 AO-BDD with 0.5 mM Fe<sup>2+</sup> (AO-BDD-Fe<sup>2+</sup>), (▲) electro-Fenton (EF) in BDD/air-diffusion  
543 electrode (ADE) cell with 0.5 mM Fe<sup>2+</sup> (EF-BDD) and (▽) AO-BDD with 0.5 mM Fe<sup>2+</sup> under  
544 UVA irradiation (AO-BDD-Fe<sup>2+</sup>-UVA). Current density of 33.3 mA cm<sup>-2</sup> in all EAOPs.

545 **Fig. 3.** Percentage of nitrogen released as (■) NH<sub>4</sub><sup>+</sup> ion, (▨) NO<sub>3</sub><sup>-</sup> ion and (□) NO<sub>x</sub>  
546 species at the end of the trials of Fig. 2b for oxamic acid.

547 **Fig. 4.** Proposed reaction sequence for the mineralization of Fe(III)-oxalate complexes in  
548 acidic aqueous medium by EAOPs with Fe<sup>2+</sup> as catalyst under UVA irradiation using a BDD  
549 anode.

550 **Fig. 5.** Effect of current density on (a) TOC removal and (b) concentration decay for the AO-  
551 BDD-Fe<sup>2+</sup>-UVA treatment of 100 mL of 2.08 mM oxamic acid in 0.05 M Na<sub>2</sub>SO<sub>4</sub> with 0.5  
552 mM Fe<sup>2+</sup> at pH 3.0 and 35 °C. Current density: (○) 16.6 mA cm<sup>-2</sup>, (□) 33.3 mA cm<sup>-2</sup>, (◇)  
553 66.6 mA cm<sup>-2</sup> and (△) 100 mA cm<sup>-2</sup>. The inset panels show: (a) the mineralization current  
554 efficiency calculated from Eq. (4) and (b) the kinetic analysis assuming a pseudo first-order  
555 reaction for oxamic acid.

556 **Fig. 6.** Evolution of the concentration of (a) ammonium and (b) nitrate ions released during  
557 the experiments of Fig. 5.

558 **Fig. 7.** (a) Effect of  $\text{Fe}^{2+}$  content on the decay of oxamic acid concentration for the AO-BDD-  
559  $\text{Fe}^{2+}$ -UVA degradation of 100 mL of 2.08 mM of the carboxylic acid in 0.05 M  $\text{Na}_2\text{SO}_4$  at pH  
560 3.0,  $33.3 \text{ mA cm}^{-2}$  and  $35 \text{ }^\circ\text{C}$ . [Oxamic acid]/ $[\text{Fe}^{2+}]$  ratio: (○) 4:1, (□) 2:1, (◇) 1:1, (△) 1:2  
561 and (▽) 1:4. (b) Percentage of nitrogen lost as (■)  $\text{NH}_4^+$  ion, (▨)  $\text{NO}_3^-$  ion and (□)  $\text{NO}_x$   
562 species vs [oxamic acid]/ $[\text{Fe}^{2+}]$  ratio at the end of these experiments.

563

564  
565  
566  
567  
568  
569  
570  
571  
572  
573  
574  
575  
576  
577  
578  
579  
580  
581  
582  
583  
584  
585  
586  
587  
588

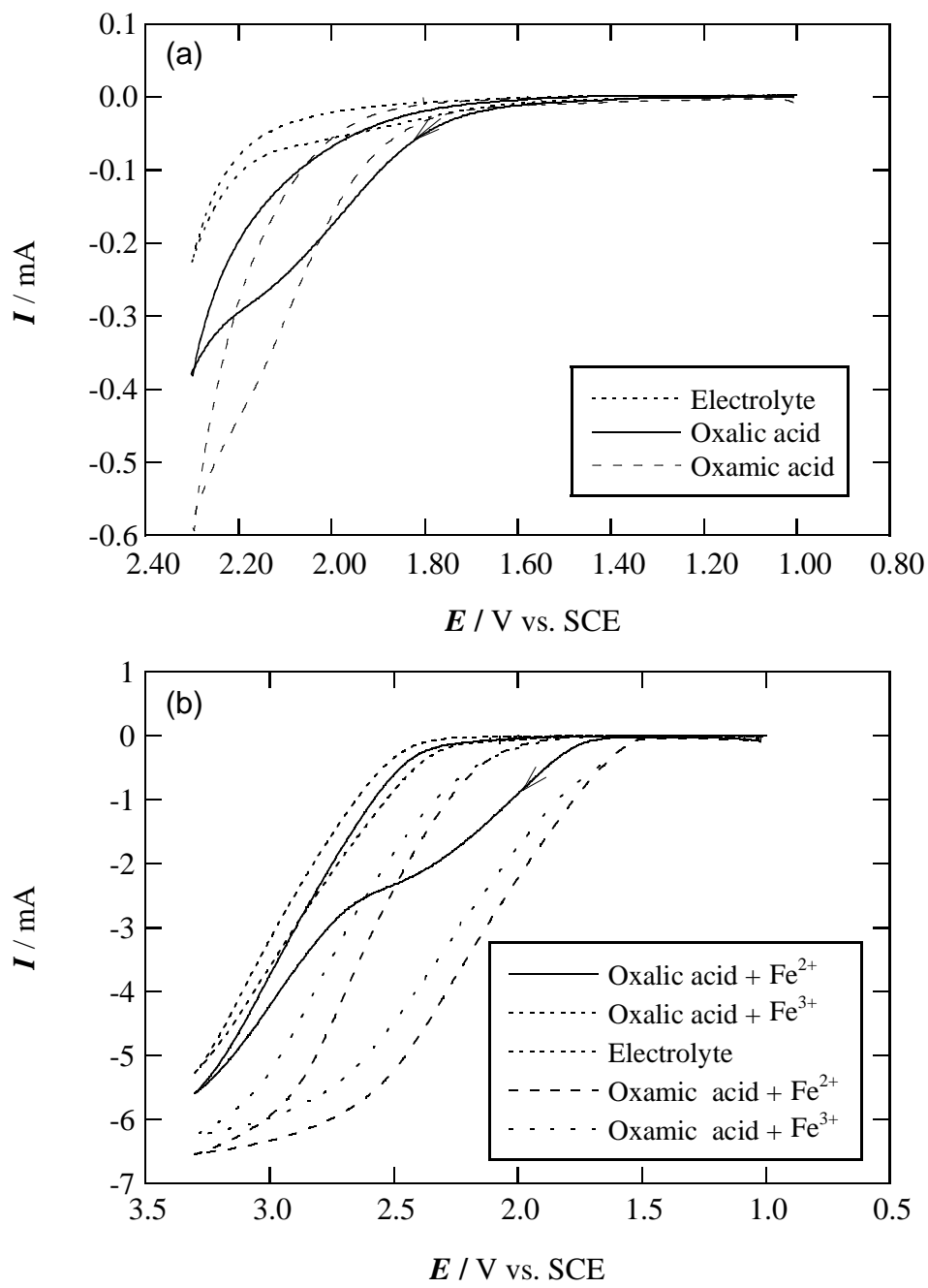


Fig. 1

589  
590  
591  
592  
593  
594  
595  
596  
597  
598  
599  
600  
601  
602  
603  
604  
605  
606  
607  
608  
609  
610  
611  
612  
613

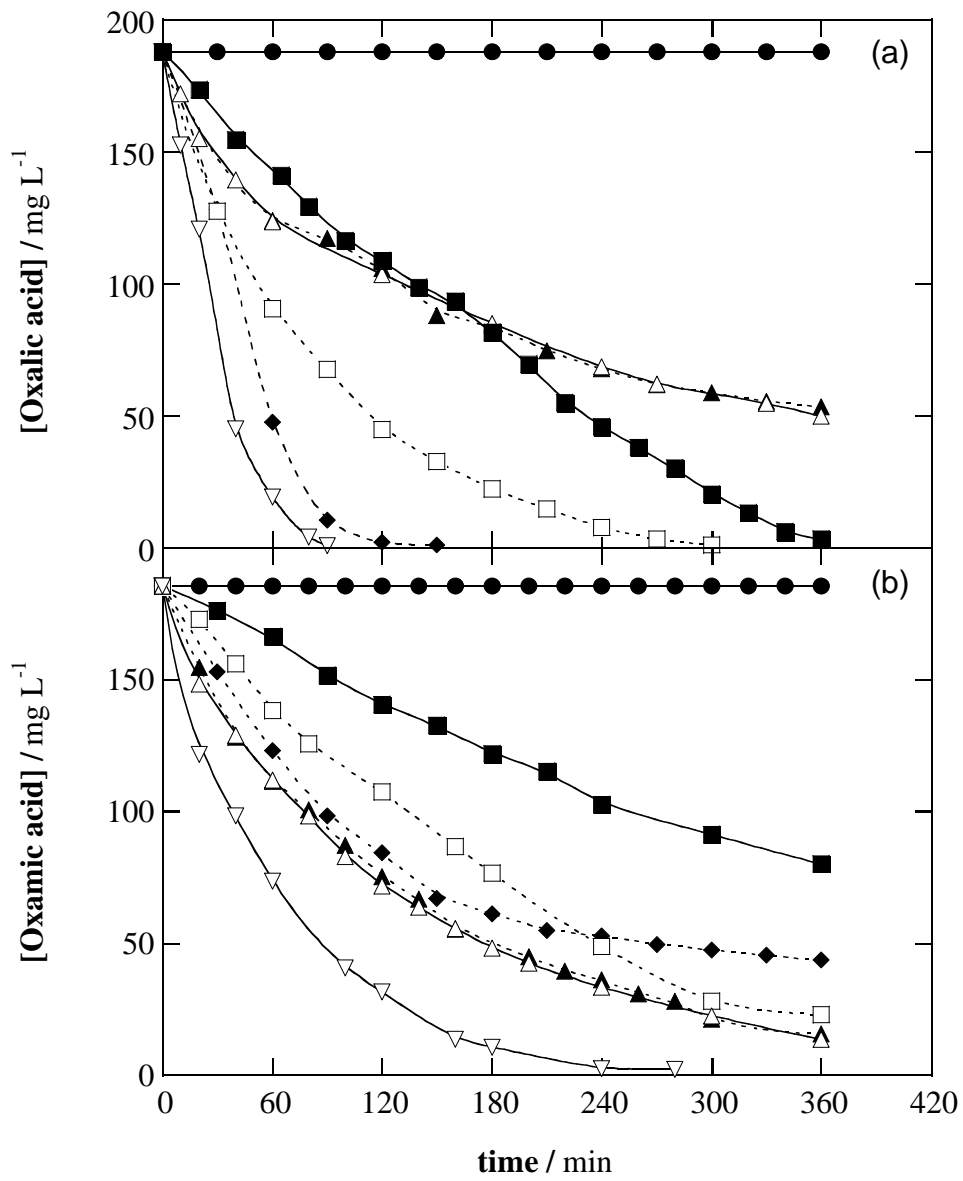


Fig. 2

614  
615  
616  
617  
618  
619  
620  
621  
622  
623  
624  
625  
626  
627  
628  
629  
630  
631  
632  
633  
634  
635  
636  
637  
638

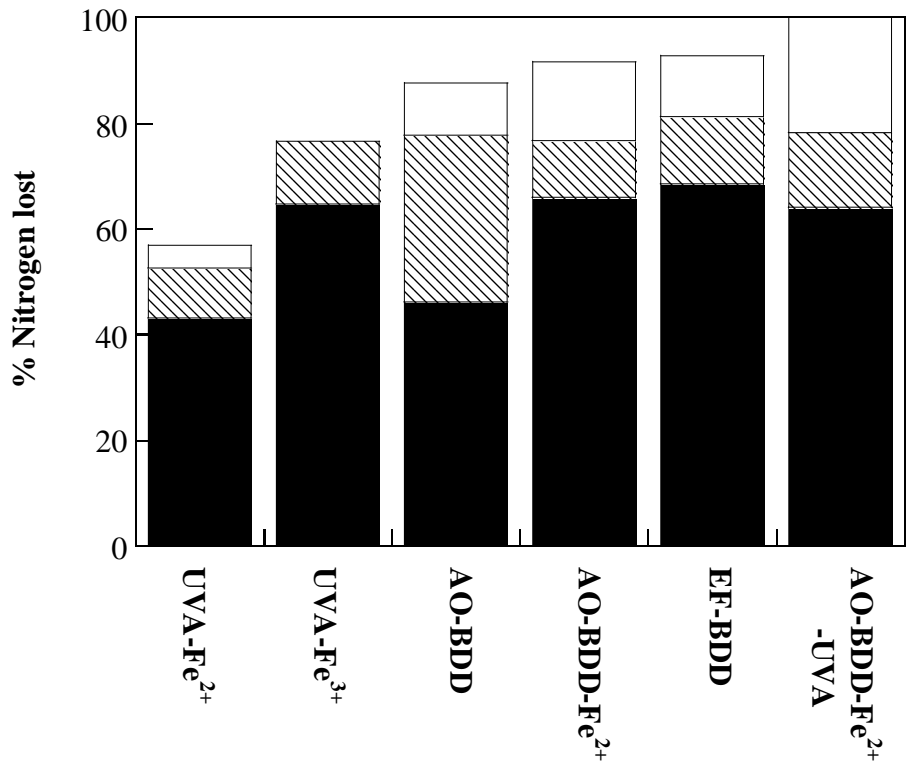


Fig. 3

639  
640  
641  
642  
643  
644  
645  
646  
647  
648  
649  
650  
651  
652  
653  
654  
655  
656  
657  
658  
659  
660  
661  
662  
663  
664  
665  
666  
667  
668  
669  
670  
671  
672  
673  
674  
675  
676  
677  
678  
679  
680  
681  
682  
683  
684  
685  
686  
687

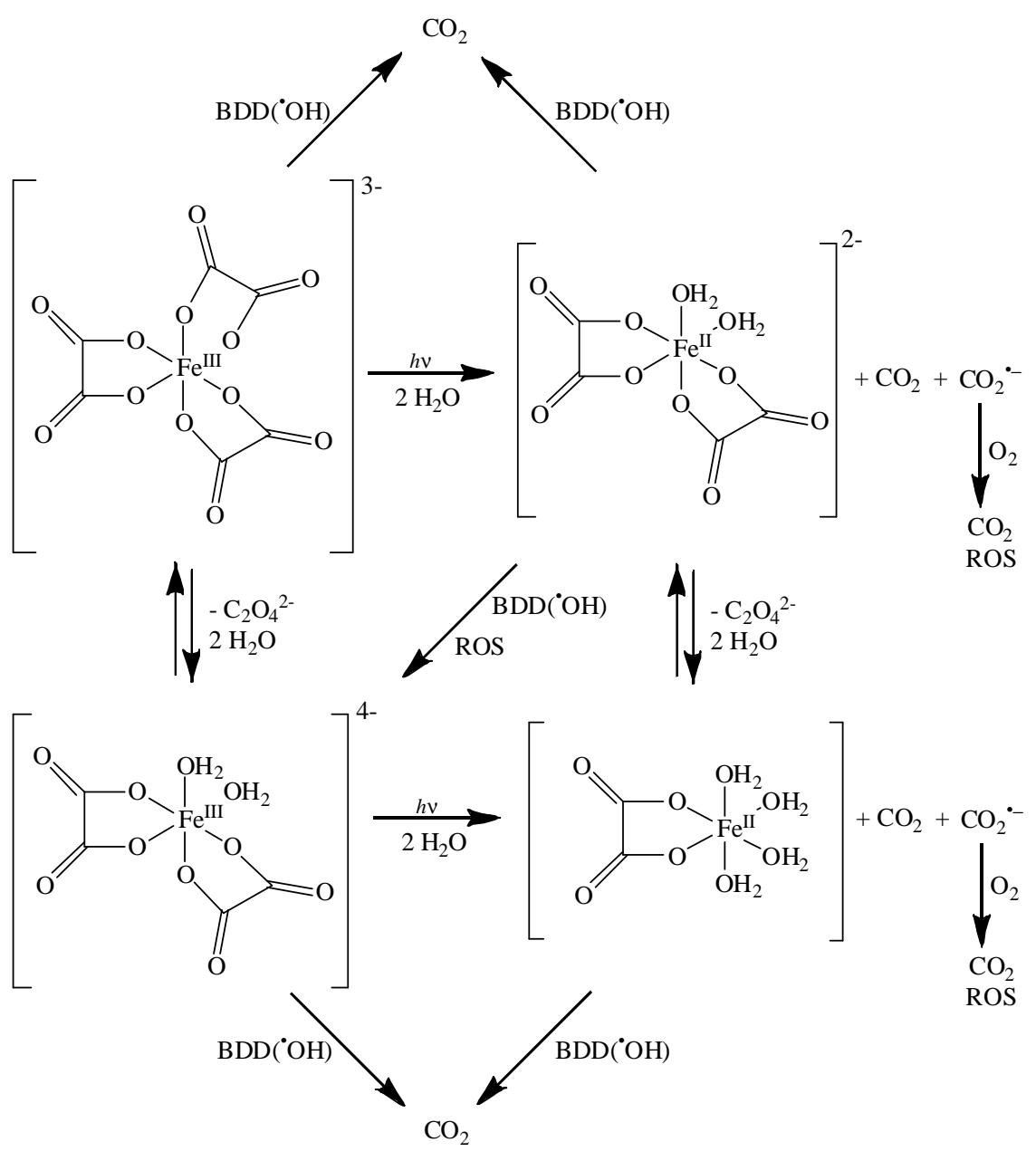
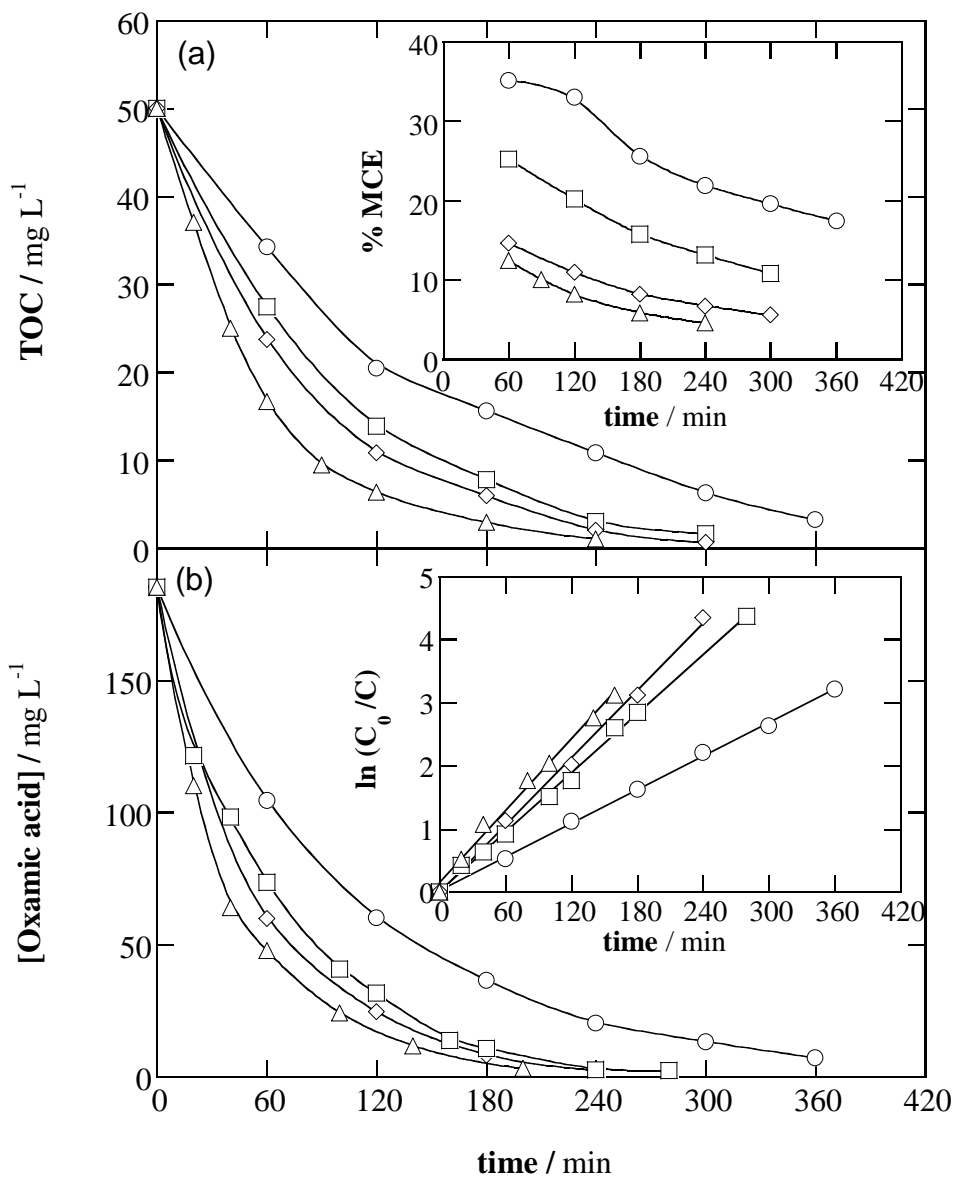


Fig. 4

688  
689  
690  
691  
692  
693  
694  
695  
696  
697  
698  
699  
700  
701  
702  
703  
704  
705  
706  
707  
708  
709  
710  
711  
712  
713



**Fig. 5**

714  
715  
716  
717  
718  
719  
720  
721  
722  
723  
724  
725  
726  
727  
728  
729  
730  
731  
732  
733  
734  
735  
736  
737  
738  
739  
740  
741  
742  
743  
744  
745  
746  
747  
748  
749  
750  
751  
752  
753  
754  
755  
756  
757  
758  
759  
760  
761  
762  
763

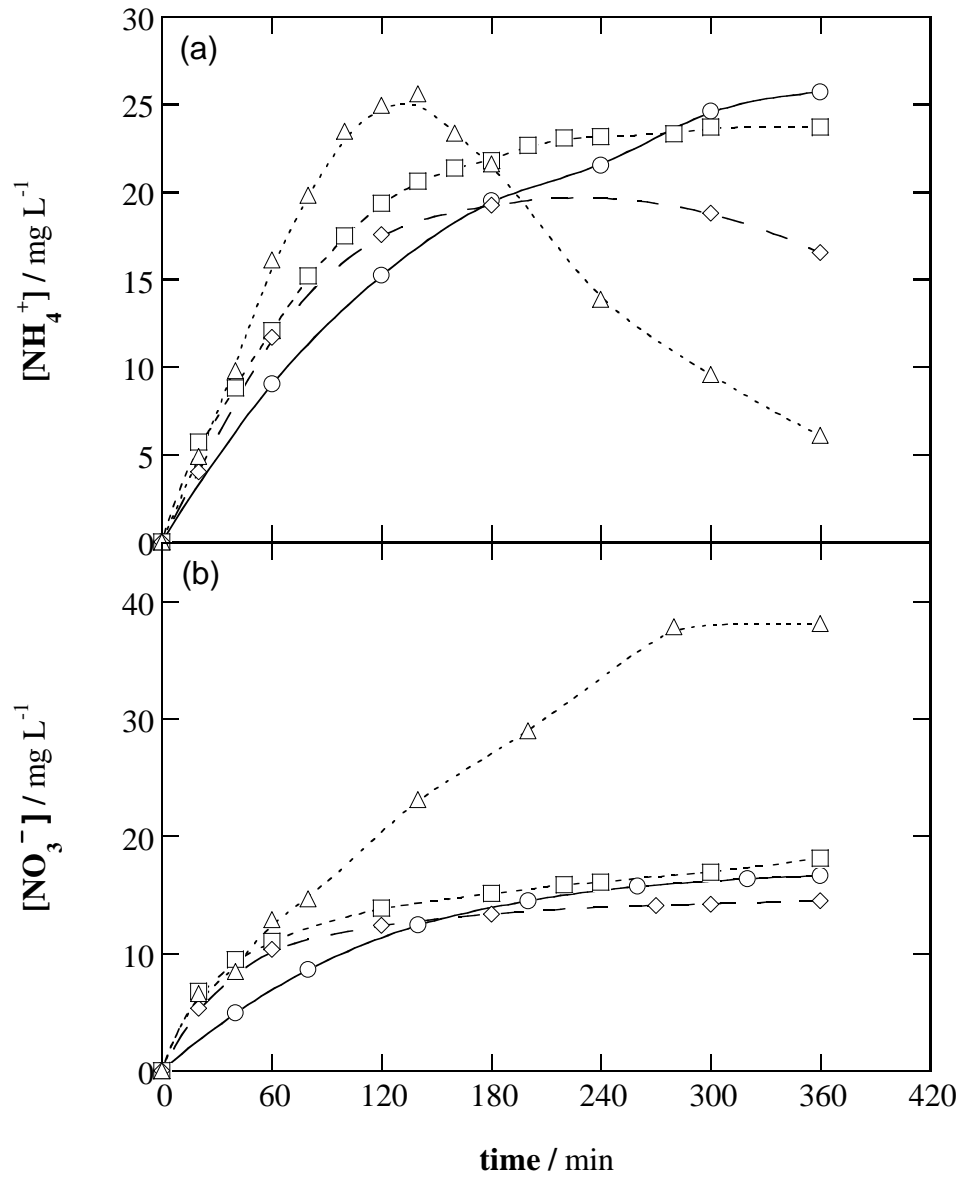


Fig. 6

764  
765  
766  
767  
768  
769  
770  
771  
772  
773  
774  
775  
776  
777  
778  
779  
780  
781  
782  
783  
784  
785  
786  
787  
788

(a)

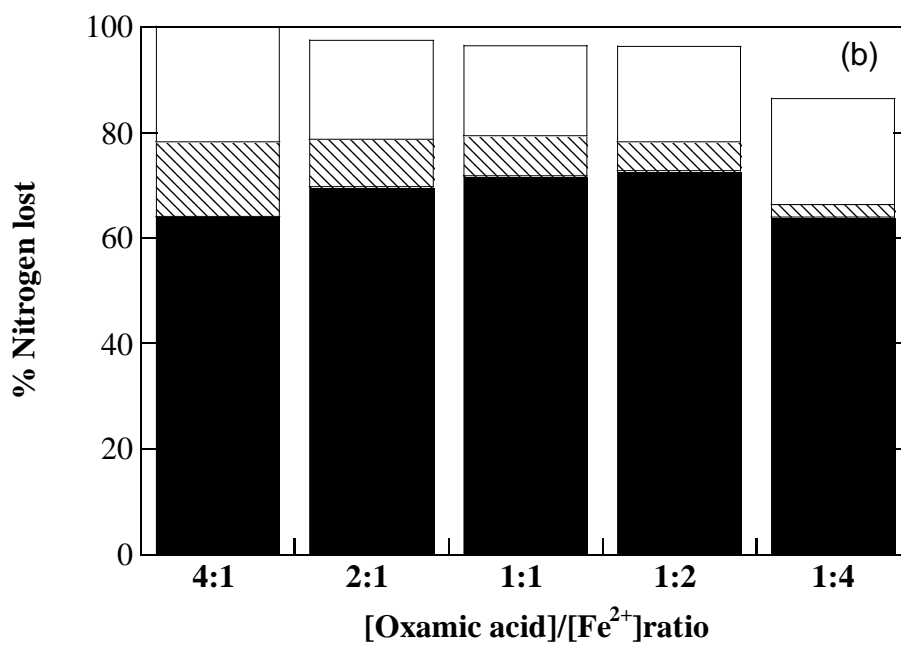


Fig. 7

789 Table 1. Pseudo first-order rate constant and square regression coefficient (in parenthesis) for  
 790 the decay of oxalic and oxamic acids during the degradation of 2.08 mM of each compound in  
 791 0.05 M Na<sub>2</sub>SO<sub>4</sub> with 0.5 mM Fe<sup>2+</sup> or 0.5 mM Fe<sup>3+</sup> of pH 3.0 at 35 °C. The solution was  
 792 irradiated with a 6 W UVA light and a current density of 33.3 mA cm<sup>-2</sup> was applied in all  
 793 EAOPs.

Method	$k_{\text{oxalic}} \times 10^4 \text{ (s}^{-1}\text{)}$	$k_{\text{oxamic}} \times 10^4 \text{ (s}^{-1}\text{)}$
UVA-Fe <sup>2+</sup>	0.75 (0.995)	0.40 (0.978)
UVA-Fe <sup>2+</sup> (O <sub>2</sub> sat.)	1.33 (0.988)	--- <sup>a</sup>
UVA-Fe <sup>3+</sup>	6.43 (0.985)	1.10 (0.996)
UVA-Fe <sup>3+</sup> (O <sub>2</sub> sat.)	6.83 (0.984)	--- <sup>a</sup>
AO-BDD	1.49 (0.999)	1.01 (0.993)
AO-BDD-Fe <sup>2+</sup>	0.61 (0.986)	1.20 (0.998)
EF-BDD-Fe <sup>2+</sup>	0.61 (0.989)	1.15 (0.998)
AO-BDD-Fe <sup>2+</sup> -UVA	9.01 (0.983)	2.82 (0.995)

<sup>a</sup>Not determined

795

796

797

798

799

800

801

802

803

804

805 Table 2. Pseudo first-order rate constant and square regression coefficient (in parenthesis)  
 806 determined for the decay of oxamic and oxalic acids during the degradation of 100 mL  
 807 solutions of different percentages of oxamic acid with a total acid concentration of 2.08 mM  
 808 by several EAOPs at 33.3 mA cm<sup>-2</sup>.

809  
 810

% Oxamic acid	AO-BDD		AO-BDD-Fe <sup>2+</sup>		AO-BDD-Fe <sup>2+</sup> -UVA	
	$k_{\text{oxamic}} \times 10^4$ (s <sup>-1</sup> )	$k_{\text{oxalic}} \times 10^4$ (s <sup>-1</sup> )	$k_{\text{oxamic}} \times 10^4$ (s <sup>-1</sup> )	$k_{\text{oxalic}} \times 10^4$ (s <sup>-1</sup> )	$k_{\text{oxamic}} \times 10^4$ (s <sup>-1</sup> )	$k_{\text{oxalic}} \times 10^4$ (s <sup>-1</sup> )
43	1.05 (0.989)	1.53 (0.998)	1.33 (0.987)	1.03 (0.995)	2.27 (0.992)	7.65 (0.990)
25	1.12 (0.997)	1.54 (0.996)	1.27 (0.989)	0.97 (0.980)	2.00 (0.999)	7.62 (0.993)
8	1.12 (0.993)	1.50 (0.998)	1.36 (0.991)	0.72 (0.988)	1.61 (0.993)	7.90 (0.981)

811